ACS OMEGA

Open Access

http://pubs.acs.org/journal/acsodf

Article

Inhibition of DLL4/Notch Signaling Pathway Promotes M2 Polarization and Cell Proliferation in Pulmonary Arterial Hypertension

Guangxing Tan,[#] Chenxia Juan,[#] Yan Mao,[#] Gang Xue, and Zhuyuan Fang*

Cite This: *ACS Omega* 2024, 9, 37923−37933

Read Online

ACCESS | Metrics & More | Article Recommendations

ABSTRACT: In this study, we conducted a comprehensive analysis to identify key genes and pathways associated with pulmonary arterial hypertension (PAH) and investigated the role of delta-like ligand 4 (DLL4) in PAH pathogenesis. Through integrated analysis of multiple data sets, we identified 6 candidate differentially expressed genes (DEGs), notably *DLL4*, which showed the highest distinguishing efficiency between PAH and control samples. Functional and pathway enrichment analyses revealed the involvement of *DLL4* in critical biological processes and pathways related to PAH, including notch signaling, immune cell function, and inflammatory responses. Further investigation demonstrated that decreased *DLL4* expression correlated with increased M2 macrophage polarization, suggesting a potential role for *DLL4* in preventing M2 differentiation. Additionally, the DLL4/Notch1 axis was found to influence the Notch profile and regulate signaling mediators during M2 differentiation. These findings highlight *DLL4* as a promising biomarker and therapeutic target for PAH, shedding light on the underlying molecular mechanisms and providing insights for the development of novel treatment strategies.

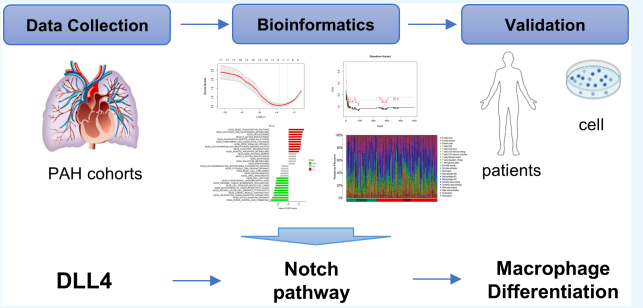

INTRODUCTION

Pulmonary arterial hypertension (PAH) is a severe cardiovascular condition characterized by increased pulmonary arterial pressure, often leading to right heart failure and mortality.[1] Despite advancements in symptomatic management, PAH remains incurable, emphasizing the urgent need for a deeper understanding of its pathogenesis to develop effective therapies.

PAH is marked by irreversible pulmonary vascular remodeling, involving endothelial cells, smooth muscle cells, and fibroblasts.[2] Notably, perivascular inflammation, characterized by the presence of various immune cells, plays a crucial role in this process.[2] Specific macrophage subtypes, particularly M1 and M2, are implicated in PAH progression.[3] M1 macrophages exacerbate inflammation, while M2 macrophages contribute to tissue repair and vascular remodeling. Concurrently, there is an increase in pro-inflammatory cytokines such as IL-1β, IL-6, IL-10, TGF-β, and TNF-α.[4,5]

Notch signaling has emerged as a key regulator of macrophage polarization.[6] DLL4, a Notch ligand predominantly expressed in endothelial and myeloid cells, plays a crucial role in endothelial−macrophage interactions during angiogenesis.[7] Notch activation in monocytes, facilitated by endothelial *DLL4*, promotes the proinflammatory M1 phenotype.[8] Recent research highlights the pivotal role of DLL4/Notch signaling in macrophage polarization. DLL4 activates Notch receptors on the macrophages, influencing their polarization toward either pro-inflammatory M1 or anti-inflammatory M2 phenotypes, crucial for immune responses and tissue homeostasis.[9,10] This pathway regulates cytokine expression, phagocytic activity, and metabolic reprogramming, offering promising avenues for immunomodulatory therapies.[11] Currently, research on the role of DLL4/Notch signaling in PAH and its molecular mechanisms in macrophage polarization remain limited. There is a notable gap in understanding how this pathway contributes to macrophage polarization and its effect on PAH pathogenesis. Further investigation is needed to elucidate the specific molecular interactions and signaling cascades involved, which could provide insights into potential therapeutic strategies targeting immune dysregulation in PAH.

Our study explores the impact of *DLL4* on macrophage differentiation, particularly its potential to disrupt M2 polarization in PAH. We propose that DLL4 orchestrates a Notch-dependent selection process, driving macrophage differentiation

Received: May 6, 2024
Revised: August 4, 2024
Accepted: August 9, 2024
Published: August 26, 2024

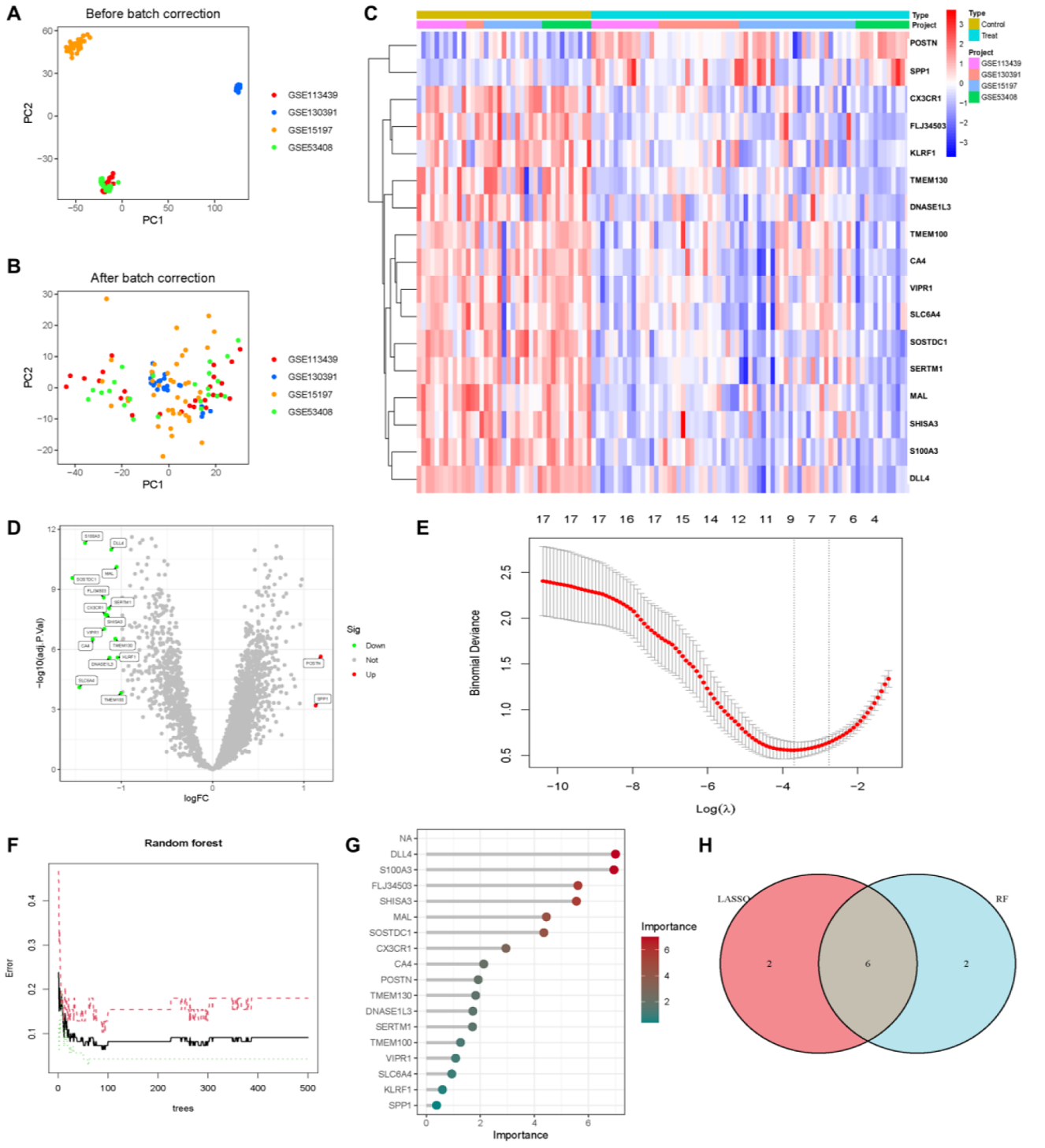

Figure 1. Candidate DEGs between PAH and control group in the training data sets. (A) PCA diagram of GSE15197, GSE53408, GSE113439, and GSE130391 data sets before calibration. (B) PCA diagram of these training data sets after calibration. (C) Heatmap of DEGs. The red and blue areas represent the significantly up- and down-regulated DEGs, respectively. (D) Volcano plot of DEGs. These genes consist of 2 upregulated genes and 15 downregulated genes. (E) Identification of the optimal penalization coefficient lambda (λ) in the LASSO model. (F) The influence of the number of decision trees on the error rate. The *x*-axis represents the number of decision trees, and the *y*-axis indicates the error rate. (G) Results of the Gini coefficient method in the RF model. The *x*-axis indicates the genetic variable, and the *y*-axis represents the importance index. (H) Venn plot exhibiting reliable biomarkers between LASSO and RF.

toward M1 while inhibiting M2 differentiation, thus contributing to PAH pathogenesis. This study sheds light on the intricate interplay among Notch signaling, inflammation, and macrophage polarization in PAH, offering insights into potential therapeutic targets for the disease.

METHODS AND MATERIALS

Microarray Data and Processing. Microarray data sets, including GSE15197, GSE53408, GSE113439, GSE130391, and GSE24988, were acquired from the GEO database. GSE15197, GSE53408, GSE113439, and GSE130391 were

https://doi.org/10.1021/acsomega.4c04307
ACS Omega 2024, 9, 37923−37933

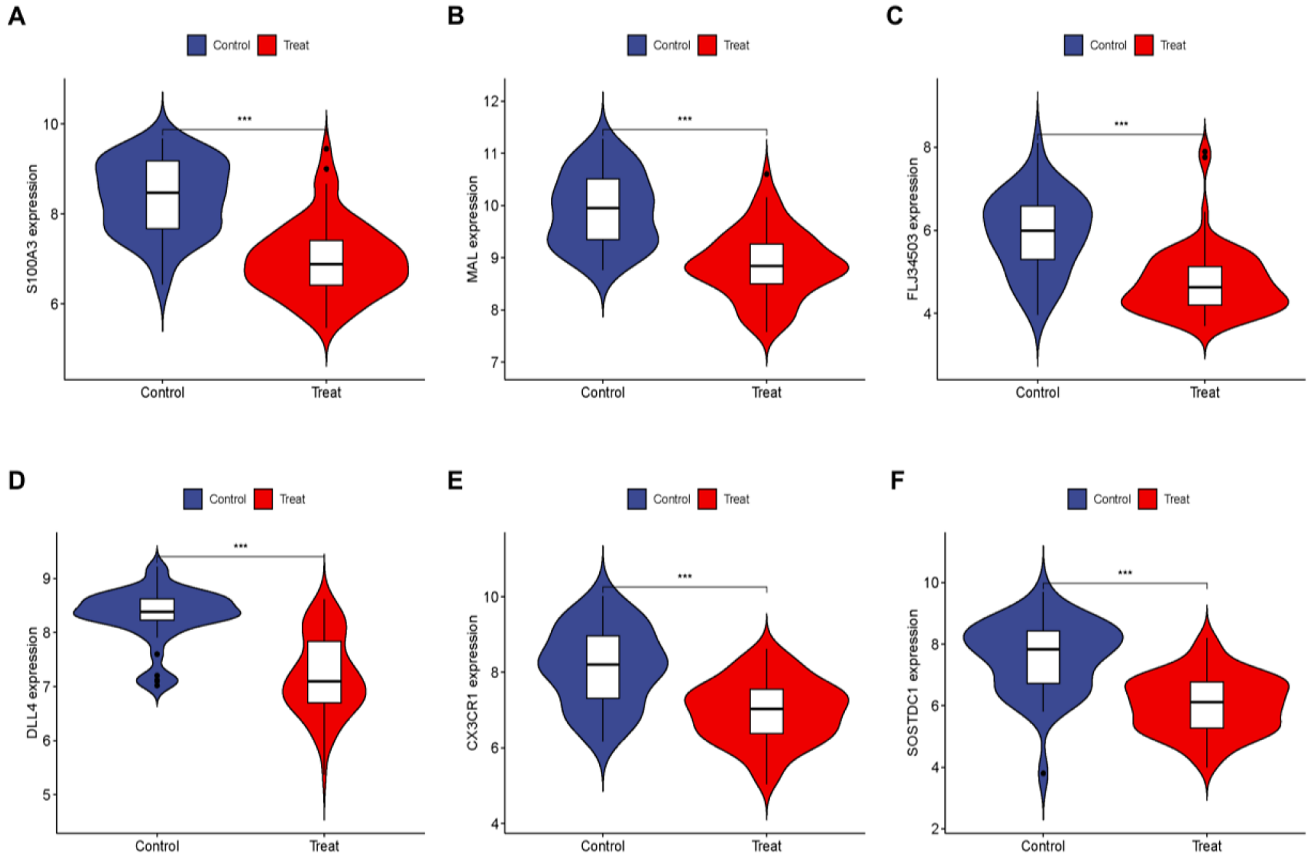

Figure 2. Expression of the identified candidate DEGs between PAH and the control group. (A−F) Violin chart for the differential expression analysis of the 6 candidate DEGs in the integrative training cohort. The blue indicates the control group, and the red represents the PAH group. $p < 0.05$ was considered statistically significant.

merged for training, while GSE24988 served as the test set. Probe names in the data sets were converted to gene names using R (version 4.1.0). After integration, the training data set comprised 39 control and 71 PAH samples. Data underwent log 2 transformation for large values and averaging for repeated probes. Batch effects were corrected using the "sva" package. Principal component analysis (PCA) plots were generated using the ggplot2 package to visualize the batch effect correction.

Screening for Candidate Differentially Expressed Genes (DEGs). The "limma" package was utilized to identify DEGs from the integrated data of GSE15197, GSE53408, GSE113439, and GSE130391. DEGs were screened based on criteria of |log 2 FC| > 1 and adjusted-p < 0.05. Heatmaps and volcano plots of DEGs were generated using the "pheatmap" and "ggplot2" packages, respectively. Machine learning analysis was conducted on DEGs to identify feature genes for PAH. A LASSO model was constructed using the "glmnet" package with parameter tuning via 10-fold cross-validation, setting the response type as binomial and α as 1. Feature genes were selected based on minimum error. The "randomForest" package was employed to establish an RF model, determining the number of trees with the minimum error. Candidate DEGs were further screened using a Venn diagram generated with the "ggvenn" R package.

Verification of the Identified Candidate DEGs. Violin plots were created using the geom-violin function from the ggplot2 R package to visualize expression patterns of identified candidate DEGs between PAH and the control samples. The "pROC" package was employed to generate receiver operating characteristic (ROC) curves for validating the DEG accuracy. Performance metrics, such as classification sensitivity, specificity, and area under the curve (AUC) were assessed. Additionally, the expression of biomarker DLL4 was validated in the external testing cohort, GSE24988.

Functional Analyses. To explore the functions regulated by *DLL4* in PAH, PAH samples were divided into two subgroups based on *DLL4* expression levels: *DLL4*-high and *DLL4*-low. The "limma" package was used to identify genes differentially expressed between these subgroups, with criteria set at |log 2 FC| > 1 and adjusted-p < 0.05. Gene ontology (GO) and Kyoto encyclopedia of genes and genomes (KEGG) analyses were conducted using the "clusterProfiler" R package to investigate potential molecular mechanisms of these genes in PAH. Single-gene gene set enrichment analysis (GSEA) was performed using the "clusterProfiler" and "enrichplot" packages, classifying samples into high and low expression groups based on median expression values. Gene set variation analysis (GSVA) was employed with the "c2.cp.kegg.Hs.symbols" subset from the MSigDB database to examine pathway variations. Pathway and biological function differences between subtypes were analyzed using the "limma" and "GSVA" packages.

Infiltration of Immune Cells and Correlation Analysis. The "CIBERSORT" algorithm was used to estimate immune cell infiltration ratios in both the PAH and control samples. Default signature matrix permutations were set to 1000, and the standard immune cell expression file (LM22.txt) was obtained from the official website. Differences in immune cell proportions between the two groups were assessed by using the Wilcoxon

https://doi.org/10.1021/acsomega.4c04307
ACS Omega 2024, 9, 37923−37933

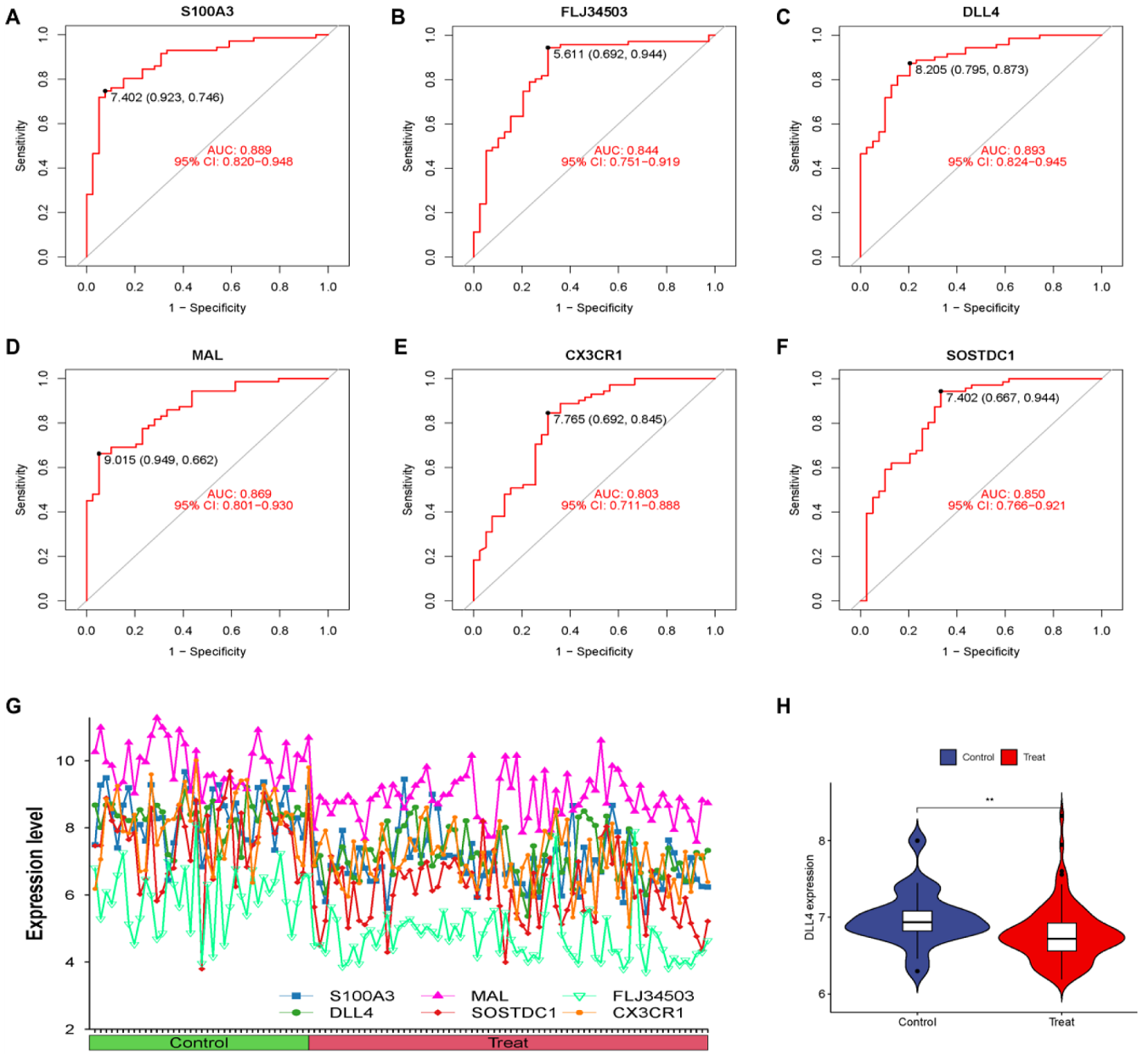

Figure 3. Verification of the identified candidate DEGs. (A−F) ROC curves for evaluating the diagnostic ability of the 6 candidate DEGs in the integrative training cohort. (G) Line chart for the expression of candidate DEGs in the integrative training cohort. Each point represented a sample. (H) Violin chart for the differential expression analysis of *DLL4* in the GSE24988 testing cohort.

rank sum test. Spearman correlation analysis was conducted to explore the relationships between candidate genes and infiltrating immune cells.

PBMC Collection and Small-Interfering RNA (siRNA) Transfection. Peripheral blood mononuclear cells (PBMCs) were collected from both non-PAH and PAH volunteers using EDTA vacutainer tubes. PBMCs were isolated using the histopaque density gradient method and a Sepmate Tube. Monocytic cells were obtained by seeding PBMCs in 6-well or 24-well plates at a density of 3×10^6 cells/well and culturing them in RPMI-1640 medium supplemented with glutamine, sodium pyruvate, HEPES, Normocin, and penicillin−streptomycin. The cells were then incubated at 37 °C with 5% CO_2 for 3 h. After removing nonadherent cells, adherent monocytes were washed with serum-free culture medium and further incubated for 24 h in RPMI with 2% fetal bovine serum.

PBMCs were cultured as previously described. Following culture, the cells were transfected with siRNAs using linear polyethylenimines (PEIs) Reagent according to the manufacturer's instructions. The siRNAs targeted DLL4 or were scrambled (control) siRNA. The efficiency of gene knockdown was evaluated using QPCR and Western blot.

Differentiation and Polarization Protocol. Purified PBMCs were cultured in RPMI1640 medium supplemented with 20% fetal bovine serum (FBS), glutamine, penicillin−streptomycin, nonessential amino acids, sodium pyruvate, and M-CSF (100 ng/mL) for 7 days on 9 cm^2 dishes (1.107 cells/cm2) to induce differentiation into M0 macrophages. For M1/M2 polarization, M0 macrophages (2.5×10^5 cells/cm^2) were further cultured for an additional 48 h in RPMI supplemented with 10% FBS and either IFN-γ plus LPS for M1 differentiation

https://doi.org/10.1021/acsomega.4c04307
ACS Omega 2024, 9, 37923−37933

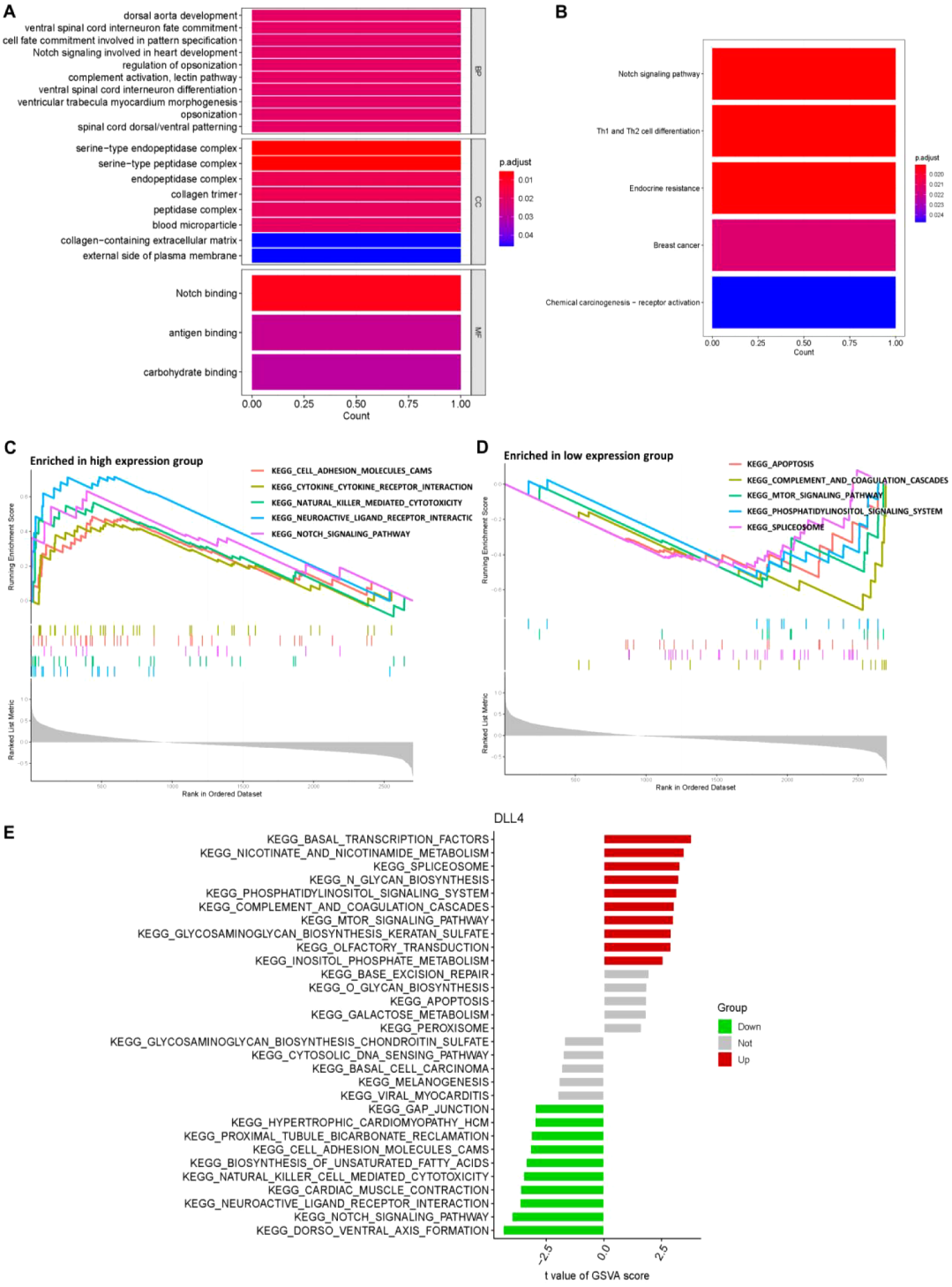

Figure 4. Function enrichment analysis. (A) Histogram exhibiting the results of the GO pathway analysis. (B) Histogram exhibiting the results of the KEGG pathway analysis. (C,D) Enrichment plots from GSEA analysis in the *DLL4*-high subgroup (C) and *DLL4*-low subgroup (D). (E) Histogram exhibiting the results of the GSVA analysis.

or with IL-4 for M2a differentiation, or IL-10 for M2c differentiation.

Statistical Analysis. Experiments were performed in triplicate to ensure reproducibility. Data are expressed as mean ± standard deviation (SD) and analyzed using non-parametric Mann−Whitney test and Kruskal−Wallis test (with Dunn's multiple comparison post-test) for comparisons involving multiple conditions. A $p < 0.05$ was considered statistically significant. In figures, (*) indicates $p < 0.05$, (**) indicates $p < 0.01$, and (***) indicates $p < 0.005$.

RESULTS

The Candidate DEGs Between PAH and Control Groups in the Training Data Sets. The GSE15197, GSE53408, GSE113439, and GSE130391 data sets were integrated and underwent batch calibration to mitigate batch effects. Principal component analysis (PCA) was employed to

https://doi.org/10.1021/acsomega.4c04307
ACS Omega 2024, 9, 37923−37933

assess the effectiveness of this calibration (Figure 1A,B). Subsequently, to identify differentially expressed genes (DEGs) between PAH and control samples, a Bayesian test was conducted on the training data set, yielding a total of 17 DEGs, comprising 2 upregulated and 15 downregulated genes (Figure 1C,D). Machine learning analysis was then carried out on these 17 DEGs using R software. LASSO feature selection identified 8 genes (Figure 1E), while 8 genes with importance values exceeding 2 were chosen as disease-specific genes in the Random Forest (RF) model (Figure 1F,G). Finally, Venn analysis yielded 6 candidate DEGs (Figure 1H).

Verification of the Identified Candidate DEGs. Compared with control samples, decreased *S100A3*, *DLL4*, *MAL*, *SOSTDC1*, *FLJ34503*, and *CX3CR1* expression were observed in the PAH samples from the integrative training cohort (Figure 2A−F). To estimate the predictive utility, the ROC curve was performed and it was found that the *S100A3*, *DLL4*, *MAL*, *SOSTDC1*, *FLJ34503*, and *CX3CR1* illustrated a remarkably distinguishing efficiency with AUC values of 0.889 (95% CI: 0.820−0.948), 0.893 (95% CI: 0.824−0.945), 0.869 (95% CI: 0.801−0.930), 0.850 (95% CI: 0.766−0.921), 0.844 (95% CI: 0.751−0.919), and 0.803 (95% CI: 0.711−0.888) in the integrative training cohort, respectively (Figure 3A−F). It was obvious that the *DLL4* gene showed the highest distinguishing efficiency in the 6 candidate DEGs. Line chart in Figure 3G showed the expression levels of the 6 identified genes in the training set. Interestingly, the results were validated in the GSE24988 cohort, and a consistent gene expression pattern of *DLL4* was obtained (Figure 3H). Hence, we chose *DLL4* as the biomarker for PAH patients.

Function and Pathway Enrichment Analysis on PAH Based on *DLL4*. Genes exhibiting differential expression between the *DLL4*-high and *DLL4*-low subgroups were subjected to functional pathway analysis. This analysis revealed involvement in various biological processes, including dorsal aorta development, regulation of opsonization, complement activation of the lectin pathway, notch signaling in heart development, and ventricular trabecula myocardium morphogenesis. Regarding cellular components, the focus was on peptidase complexes. Molecular function analysis highlighted genes associated with notch binding, antigen binding, and carbohydrate binding (Figure 4A). Additionally, KEGG pathway enrichment identified the notch signaling pathway, Th1 and Th2 cell differentiation, endocrine resistance, and chemical carcinogenesis-receptor activation, among others (Figure 4B).

Further single-gene GSEA analysis delineated enrichment of cell adhesion molecules, cytokine receptor interaction, natural killer cell-mediated cytotoxicity, neuroactive ligand receptor interaction, and the notch signaling pathway in the DLL4-high subgroup (Figure 4C). Conversely, apoptosis, complement, and coagulation cascades, the mTOR signaling pathway, the phosphatidylinositol signaling system, and the spliceosome were enriched in the DLL4-low subgroup (Figure 4D). Moreover, GSVA enrichment analysis implicated the mTOR signaling pathway, basal transcription factors, cell adhesion molecules, natural killer cell-mediated cytotoxicity, and notch signaling pathway in the pathogenesis of *DLL4*-associated PAH (Figure 4E).

Estimation of Infiltrating Immune Cells and Correlation Analysis. We began by estimating the proportions of 22 infiltrating immune cells using the "CIBERSORT" algorithm on the gene matrix of 28 samples. Compared to control samples, PAH samples exhibited significantly lower proportions of CD8 T cells, CD4 memory activated T cells, and M2 macrophages, while proportions of resting dendritic cells, activated dendritic cells, eosinophils, and neutrophils were significantly higher (Figure 5A). The composition of infiltrating immune cells in PAH and control samples is depicted in Figure 5B. Pearson's correlation coefficient analysis revealed strong correlations between different types of infiltrating immune cells (Figure 5C), emphasizing the importance of immune status in PAH.

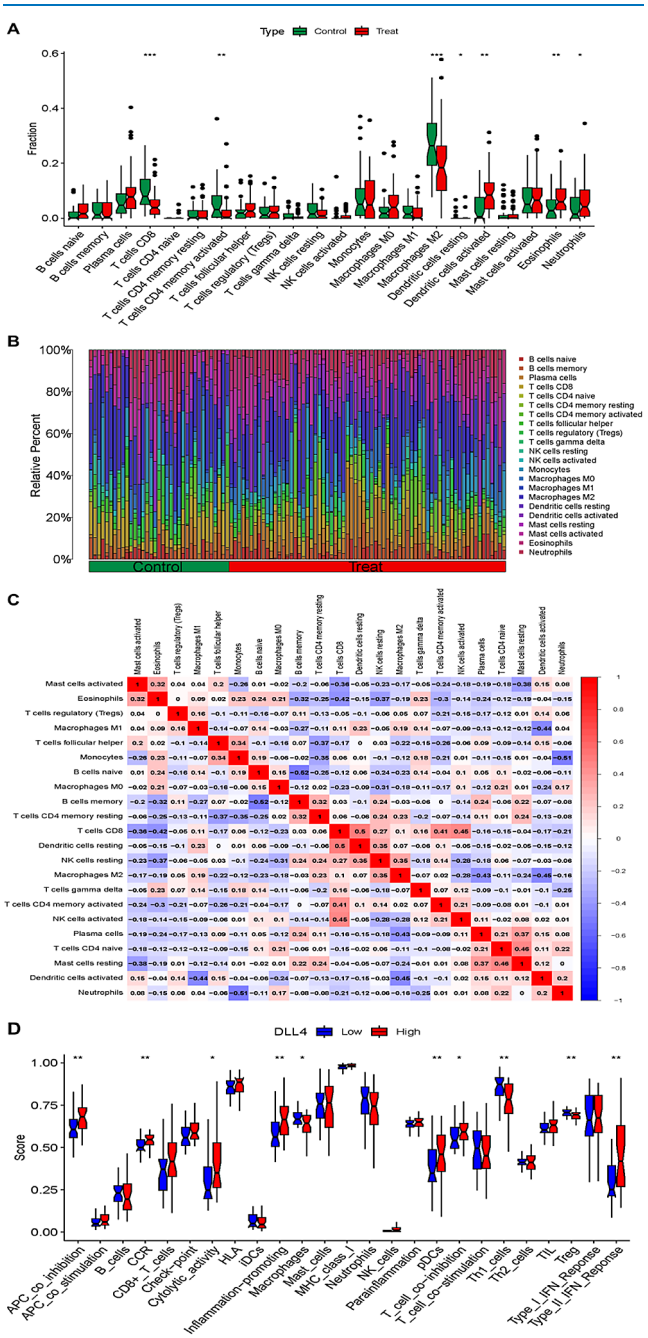

Figure 5. Infiltration of immune cells and correlation analysis. (A) Boxplots comparing the proportions of 22 major immune cell subsets between PAH and control samples. (B) The histogram showed the distribution characteristics of immune cells in PAH. (C) Pearson's correlation coefficient revealed astrong link between each type of infiltrating immune cells. (D) Boxplots comparing the immune-related function between the *DLL4*-high subgroup and *DLL4*-low subgroup.

https://doi.org/10.1021/acsomega.4c04307
ACS Omega 2024, 9, 37923−37933

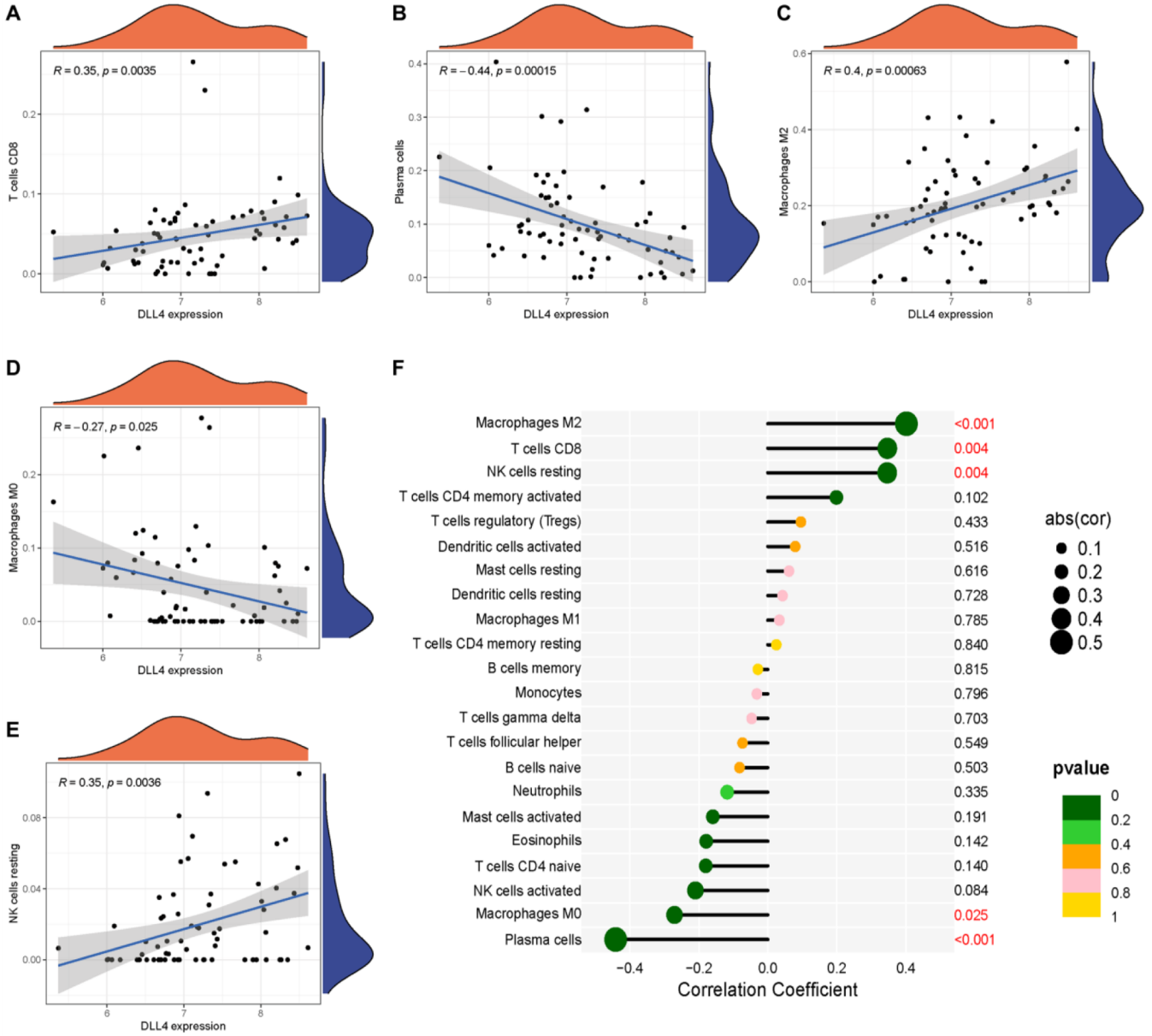

Figure 6. Correlation analysis of DLL4 and immune cells. (A–E) Spearman correlation analyses between *DLL4* expression levels in the PAH samples and the infiltrations of five kinds of immune cells, including CD8 T cells (A), plasma cells (B), M2 macrophages (C), M0 macrophages (D), and resting NK cells (E). (F) Immune infiltrating cells associated with *DLL4* in PAH.

To delve deeper into the immune−*DLL4* gene relationship in PAH, we analyzed the immune functions between two PAH subgroups stratified by *DLL4* expression. This analysis identified 10 significant immune functions, including APC coinhibition, type II IFN response, T cell coinhibition, pCDs, inflammation promoting, CCR, cytolytic activity, macrophages, Th1 cells, and Tregs (Figure 5D). Figure 6A–F further confirmed positive correlations between *DLL4* expression levels and CD8 T cells (Figure 6A), M2 macrophages (Figure 6C), and resting NK cells (Figure 6E), while negative correlations were observed with plasma cells (Figure 6B) and M0 macrophages (Figure 6D) in PAH.

***DLL4* May Drive the Notch-Dependent Process and Prevent M2 Macrophage Differentiation in PAH.** We collected the peripheral blood of 47 patients diagnosed with PAH and 46 healthy controls from Jiangsu Provincial Hospital of Traditional Chinese Medicine from August 2021 to July 2023. In order to further clarify the expression of *DLL4* in PAH patients and its effect on the notch pathway in M2 macrophages, we detected the RNA expression levels of *DLL4*, notch pathway, and the molecular markers on the surface of M2 macrophages in peripheral blood mononuclear cells of PAH and control groups. We observed significantly lower expression levels of *DLL4* (**p = 0.0076) and Notch1 (**p = 0.0087) in the PAH group compared to those in the healthy control group (Figure 7A and Figure 7B). Furthermore, our investigation included the assessment of molecular markers, such as CD40, CD64, CD80, and CD86 on the surface of M1 macrophages, as well as CD11b (**p = 0.0065), CD200R (**p = 0.0089), CD163 (*p = 0.0223,) and CD206 (*p = 0.0342) on the surface of M2 macrophages. Our findings revealed a notably higher presence of M2 macrophages in the PAH group compared with the control group (Figure 7C).

https://doi.org/10.1021/acsomega.4c04307
ACS Omega 2024, 9, 37923−37933

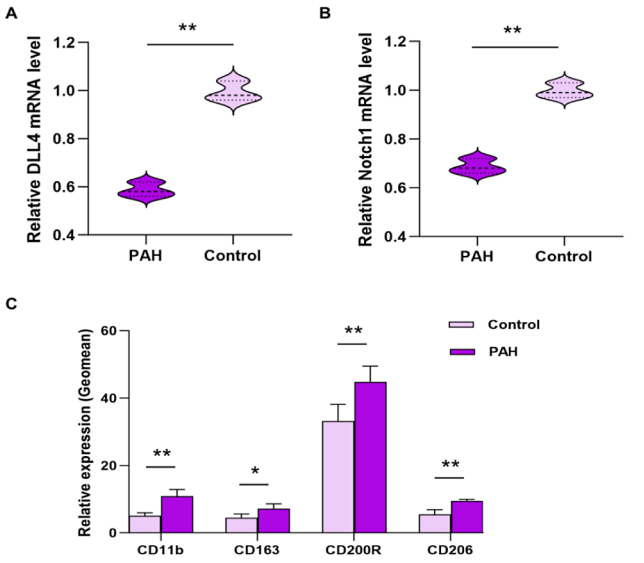

Figure 7. *DLL4* may drive the Notch-dependent process and prevent M2 macrophage differentiation in PAH. (A) and (B) *DDL4* and Notch expression levels in PAH patients (n = 47) and healthy controls (n = 46). (C) The expression levels of the molecular markers (CD11b, CD200R, and CD206) of M2 macrophages in PAH and healthy controls.

Decreased *DLL4* Facilitates IL-4-Driven Differentiation into M2 Macrophages. To explore the interaction between *DLL4* and the macrophage phenotype, monocytes from healthy volunteers were isolated and differentiated into M0 macrophages using M-CSF for 7 days. Subsequently, polarization into M1 macrophages with IFN-γ and LPS, or into M2 macrophages (specifically M2a subtype) using IL-4 for 48 h, was conducted as previously outlined. The phenotype of M1 and M2 macrophages at 24 h postdifferentiation, compared to M0 macrophages harvested at the end of M-CSF treatment, is depicted in Figure 8A.

Under these conditions, polarized M1 macrophages exhibited significant phenotypic changes compared to M0, including notably increased expression of CD40 and CD86, along with a trend toward elevated CD80. Conversely, LPS/IFN-γ treatment induced no changes in M2 markers. Polarization in the presence of IL-4 resulted in increased expression of three of four tested M2-specific markers (CD11b, CD200R, and CD206), with no impact on the M1 markers.

To investigate the impact of *DLL4* on macrophage polarization, we evaluated the expression of surface molecular markers on each macrophage subtype after *DLL4* knockdown. As shown in Figure 8B, *DLL4* was knocked down successfully (**p = 0.0017). We observed a significant increase in the expression of CD11b (**p = 0.0085), CD206 (**p = 0.0039), and CD200R (**p = 0.0057) upon IL-4 stimulation following *DLL4* knockdown (**p = 0.0035, Figure 8C) and a significant decrease in the expression of *Notch1* (**p = 0.0031, Figure 8D). Importantly, *DLL4* knockdown did not alter the basal expression of CD11b, CD206, or CD200R on M0 or M1 macrophages.

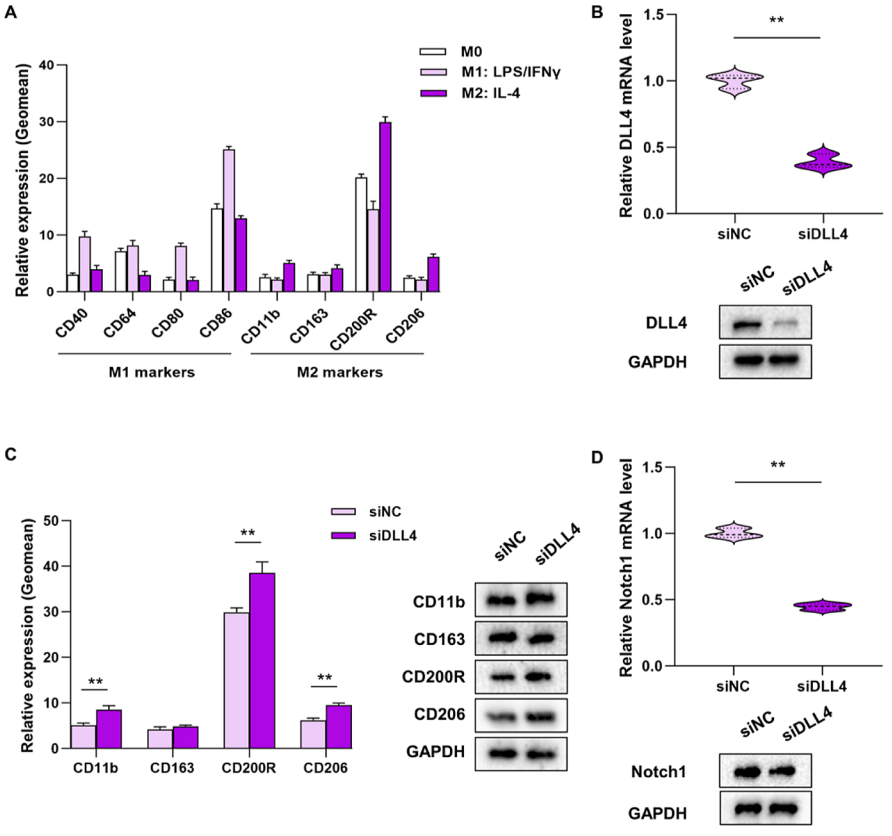

Figure 8. Reduced *DLL4* promotes IL-4-mediated differentiation into the M2 macrophage. (A) Phenotype analysis of macrophages before (M0) and after polarization in M1 or M2 macrophages for 24 h with LPS and IFN-γ or IL-4, respectively. (B) The mRNA and protein expression levels of *DLL4* upon IL-4 stimulation following *DLL4* knockdown. (C) The mRNA and protein expression of *CD11b*, *CD206*, and *CD200R* upon IL-4 stimulation following *DLL4* knockdown. (D) The mRNA and protein expression of *Notch1* upon IL-4 stimulation followed *DLL4* knockdown.

https://doi.org/10.1021/acsomega.4c04307
ACS Omega 2024, 9, 37923−37933

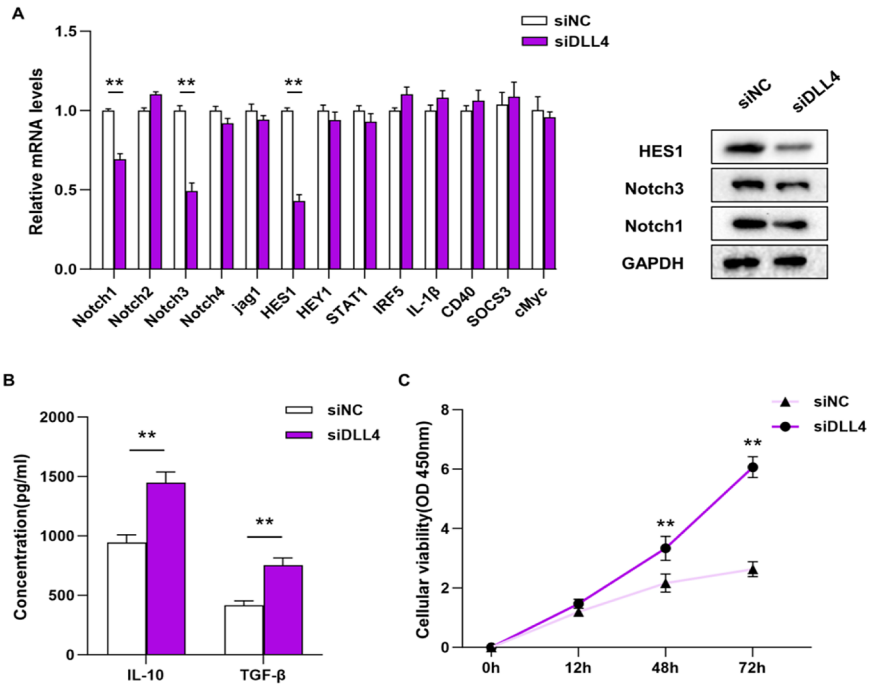

Figure 9. DLL4/Notch1 axis influences the Notch profile and regulates signaling mediators upon M2 differentiation. (A) Upon M2 polarization knocked-down *DLL4* decreased mRNA and protein levels for Notch1, Notch3, and HES. (B) The levels of inflammatory factors (IL-10 and TGF-β) released by M2 cell. (C) The cell proliferation level increased after knocking down *DLL4* detected by the CCK-8 kit.

Furthermore, manipulating *DLL4* expression during M1 polarization did not induce significant changes in M1-specific markers (CD40, CD64, CD80, and CD86).

These results suggest an inhibitory function of *DLL4* and Notch signaling in the IL-4 signaling pathway. In summary, our data imply that Notch signaling mediated by *DLL4* acts as a regulatory mechanism in macrophage differentiation, crucially preventing M2 polarization.

The DLL4/Notch1 Axis Impacts Notch Profile and Modulates Signaling Mediators During M2 Differentiation. Quantitative RT-PCR and Western blot were employed for gene expression analysis to elucidate the regulation mediated through DLL4/Notch in M2 macrophages. Macrophages polarized with IL-4 (M2) with or without *DLL4* knockdown were analyzed. Thirteen transcripts encoding Notch receptors, ligands, effectors, and signaling molecules were detected. Our findings indicate that *DLL4* selectively influences RNA transcription and protein expression during M2 differentiation. Knockdown of *DLL4* during M2 polarization resulted in decreased mRNA levels for Notch1 ($^{**}p = 0.0065$), Notch3 ($^{**}p = 0.0077$), and HES1 ($^{**}p = 0.0089$) (Figure 9A). Further analyses showed that the protein levels of Notch1, Notch3, and HES1 were also decreased when the *DLL4* was knocked down (Figure 9A). Hence, *DLL4* appears to selectively activate the Notch pathway in macrophage subsets.

Considering that Notch signaling pathway was inhibited after DLL4 was knocked down, promoting the polarization of M2 cells, we further examined the changes in the levels of inflammatory factors released by M2 cells and found that the concentrations of IL-10 ($^{**}p = 0.0087$) and TGF-β ($^{**}p = 0.0066$) were significantly increased (Figure 9B). DLL4/Notch signaling pathway affects the polarization of M2 and the release of downstream inflammatory factors. We detected by the CCK8 kit that the cell proliferation level increased after knocking down DLL4 ($^{**}p = 0.0087$, Figure 9C).

DISCUSSION

Recent studies indicate that PAH is closely associated with pulmonary vascular remodeling[12] and immune cell[13] involvement. Immune cells, such as macrophages contribute to vascular remodeling by promoting inflammation and releasing growth factors that stimulate smooth muscle cell proliferation.[14]

The purpose of this study is to identify potential key genes and underlying mechanisms of PAH using various bioinformatics approaches. Five data sets derived from PAH patients were obtained from GEO, with one data set designated as a validation set. Utilizing multiple bioinformatics techniques, including DAVID, STRING, R language, and Cytoscape, we investigated the DEGs between PAH patients and healthy controls and conducted GO annotation and KEGG enrichment analysis. Compared with existing studies, our bioinformatics analysis results are more reflective of the actual environment. Furthermore, our immune infiltration analysis revealed that macrophages constitute the largest proportion of immune cells, differing from some previous reports that highlighted monocytes,[15] and aligning with certain other studies.[16,17] Preliminary identification of candidate DEGs between the PAH and control groups revealed 17 DEGs, with *DLL4* emerging as a promising biomarker due to its consistently reduced expression in PAH samples across multiple data sets. Subsequent validation of these candidate DEGs confirmed the downregulation of *DLL4* in PAH, consistent with sporadic reports in the existing literature.[18] Studies have indicated that restoring DLL4/Notch1/PPARγ signaling may be beneficial in preventing or reversing the pathological vascular remodeling in PAH, offering new hope for PAH treatment.[19]

Through further KEGG and immune cell infiltration analyses, we found that *DLL4* is associated with the downstream Notch signaling pathway and macrophages. While other studies have shown that DLL4/Notch signaling promotes pro-inflammatory macrophage activation and accelerates atherosclerosis in chronic

https://doi.org/10.1021/acsomega.4c04307
ACS Omega 2024, 9, 37923−37933

kidney disease,[10,20] some reports indicate that DLL4 inhibitors can alleviate chronic atherosclerosis, venous graft disease, vascular calcification, insulin resistance, and fatty liver in mice.[21] However, there are few studies investigating the mechanisms by which DLL4 and Notch signaling affects macrophage polarization in PAH.

The investigation into infiltrating immune cells in PAH revealed significant alterations in immune cell composition with implications for disease pathogenesis. The observed decrease in CD8 T cells, CD4 memory activated T cells, and M2 macrophages, coupled with increased proportions of dendritic cells, eosinophils, and neutrophils, suggests a dysregulated immune response in PAH.[22,23] Importantly, correlation analysis revealed associations between *DLL4* expression and immune cell subsets,[24−26] highlighting the potential interplay between *DLL4* and immune dysregulation in PAH.

Further characterization of *DLL4*'s role in PAH pathogenesis elucidated its impact on macrophage polarization and inflammatory signaling. Reduced *DLL4* expression was associated with enhanced M2 macrophage differentiation, which implicated *DLL4* as a negative regulator of M2 polarization. Mechanistically, *DLL4*-mediated Notch signaling was shown to modulate the expression of key inflammatory mediators,[27] thereby influencing macrophage phenotype and function in PAH.

The study results also suggest that targeting the DLL4/Notch axis in PAH holds a potential therapeutic significance. Notably, manipulating the expression of *DLL4* influences macrophage polarization and leads to significant changes in the release of inflammatory factors and cell proliferation, which are closely related to the mechanisms of vascular remodeling in PAH.[23,28,29] This underscores the therapeutic potential of modulating *DLL4*-mediated signaling pathways in the treatment of PAH.

In conclusion, this study provides comprehensive insights into the molecular mechanisms underlying PAH pathogenesis with a specific focus on the role of *DLL4* in immune dysregulation and macrophage polarization. The findings underscore the clinical relevance of DLL4 as a diagnostic biomarker and potential therapeutic target for PAH, offering promising avenues for further research and therapeutic intervention in this devastating disease.

■ ASSOCIATED CONTENT

Data Availability Statement

The data sets presented in this study can be found in online repositories (GEO, https://www.ncbi.nlm.nih.gov/geo/). This database is the source for all multiple microarrays, including GSE15197, GSE53408, GSE113439, GSE130391, and GSE24988. The data generated by cell experiments in the present study are included in the figures and/or tables of this article.

■ AUTHOR INFORMATION

Corresponding Author

Zhuyuan Fang − *Institute of Hypertension, Jiangsu Province Hospital of Chinese Medicine, Affiliated Hospital of Nanjing University of Chinese Medicine, Nanjing, Jiangsu 210029, China*; Email: fangzhuyuan@njucm.edu.cn

Authors

Guangxing Tan − *Institute of Hypertension, Jiangsu Province Hospital of Chinese Medicine, Affiliated Hospital of Nanjing University of Chinese Medicine, Nanjing, Jiangsu 210029, China; Wuxi Hospital of Traditional Chinese Medicine, Affiliated Hospital of Nanjing University of Chinese Medicine, Wuxi, Jiangsu 214045, China*; orcid.org/0009-0005-0770-6799

Chenxia Juan − *Department of Nephrology, Jiangsu Province Hospital of Chinese Medicine, Affiliated Hospital of Nanjing University of Chinese Medicine, Nanjing, Jiangsu 210029, China*

Yan Mao − *Department of Pediatrics, Jiangsu Province Hospital of Chinese Medicine, Affiliated Hospital of Nanjing University of Chinese Medicine, Nanjing, Jiangsu 210029, China*

Gang Xue − *Yangzhou Hospital of Traditional Chinese Medicine, Yangzhou, Jiangsu 225002, China*

Complete contact information is available at: https://pubs.acs.org/10.1021/acsomega.4c04307

Author Contributions

#G.T., C.J., and Y.M. contributed equally to this paper. G.T. and Z.F. conceptualized the study; C.J. and Y.M. performed data curation and analysis; G.T., C.J., and G.X. gathered the resources for the study; G.T. and C.J. wrote the original draft; C.J., Y.M., and Z.F. reviewed and edited the manuscript; Y.M. and G.X. performed the methodolgy and software runs; Z.F. supervised the entire process. All authors have read and approved the final manuscript.

Notes

The authors declare no competing financial interest.

The study was approved by the IRB of Wuxi Hospital of Traditional Chinese Medicine.

The patients provided written informed consent for the publication. Ethics approval number: 2023-073-01.

■ ACKNOWLEDGMENTS

This work was supported by the Key program of Jiangsu Chinese Medicine Clinical Medicine Innovation Center for Hypertension (grant k2021j17-1 to Z.F.), the Peak Academic Talent Project of Jiangsu Province Hospital of Traditional Chinese Medicine (grant y2021rc01 to Z. F.), the National Natural Science Foundation of China (grant 82100753 to C. J.), and the Excellent Young Doctoral Training Program of Jiangsu Province Hospital of Chinese Medicine (grant 2024QB023 to Y. M.).

■ REFERENCES

(1) Ruopp, N. F.; Cockrill, B. A. Diagnosis and Treatment of Pulmonary Arterial Hypertension: A Review. *JAMA* **2022**, *327* (14), 1379−1391.

(2) Hassoun, P. M. Pulmonary Arterial Hypertension. *N. Engl. J. Med.* **2021**, *385* (25), 2361−2376.

(3) Abid, S.; Marcos, E.; Parpaleix, A.; Amsellem, V.; Breau, M.; Houssaini, A.; Vienney, N.; Lefevre, M.; Derumeaux, G.; Evans, S.; Hubeau, C.; et al. CCR2/CCR5-mediated macrophage−smooth muscle cell crosstalk in pulmonary hypertension. *Eur. Respir. J.* **2019**, *54* (4), 1802308.

(4) de Novaes Rocha, N.; de Oliveira, M. V.; Braga, C. L.; Guimaraes, G.; de Albuquerque Maia, L.; de Araújo Padilha, G.; Silva, J. D.; Takiya, C. M.; Capelozzi, V. L.; Silva, P. L.; et al. Ghrelin therapy improves lung and cardiovascular function in experimental emphysema. *Respir Res.* **2017**, *18* (1), 185.

(5) Zawia, A.; Arnold, N. D.; West, L.; Pickworth, J. A.; Turton, H.; Iremonger, J.; et al. Altered Macrophage Polarization Induces Experimental Pulmonary Hypertension and Is Observed in Patients With Pulmonary Arterial Hypertension. *Arterioscler., Thromb., Vasc. Biol.* **2021**, *41* (1), 430−445.

(6) Chen, W.; Liu, Y.; Chen, J.; Ma, Y.; Song, Y.; Cen, Y.; et al. The Notch signaling pathway regulates macrophage polarization in liver diseases. *Int. Immunopharmacol.* **2021**, *99*, 107938.
(7) Pitulescu, M. E.; Schmidt, I.; Giaimo, B. D.; Antoine, T.; Berkenfeld, F.; Ferrante, F.; et al. Dll4 and Notch signalling couples sprouting angiogenesis and artery formation. *Nat. Cell Biol.* **2017**, *19* (8), 915−927.
(8) Ortiz-Masia, D.; Cosin-Roger, J.; Calatayud, S.; Hernandez, C.; Alos, R.; Hinojosa, J.; et al. M1Macrophages Activate Notch Signalling in Epithelial Cells: Relevance in Crohn's Disease. *J. Crohns Colitis* **2016**, *10* (5), 582−592.
(9) Pagie, S.; Gérard, N.; Charreau, B. Notch signaling triggered via the ligand DLL4 impedes M2 macrophage differentiation and promotes their apoptosis. *Cell Commun. Signal.* **2018**, *16* (1), 4.
(10) Nakano, T.; Katsuki, S.; Chen, M.; Decano, J. L.; Halu, A.; Lee, L. H.; et al. Uremic Toxin Indoxyl Sulfate Promotes Proinflammatory Macrophage Activation Via the Interplay of OATP2B1 and Dll4-Notch Signaling. *Circulation* **2019**, *139* (1), 78−96.
(11) Xing, Y.; Pan, S.; Zhu, L.; Cui, Q.; Tang, Z.; Liu, Z.; Liu, F. Advanced Glycation End Products Induce Atherosclerosis via RAGE/TLR4 Signaling Mediated-M1Macrophage Polarization-Dependent Vascular Smooth Muscle Cell Phenotypic Conversion. *Oxid. Med. Cell. Longev.* **2022**, *2022*, 1−11.
(12) Thompson, A.; Lawrie, A. Targeting Vascular Remodeling to Treat Pulmonary Arterial Hypertension. *Trends Mol. Med.* **2017**, *23* (1), 31−45.
(13) Ferrian, S.; Cao, A.; Mccaffrey, E. F.; Saito, T.; Greenwald, N. F.; Nicolls, M. R.; et al. Single-Cell Imaging Maps Inflammatory Cell Subsets to Pulmonary Arterial Hypertension Vasculopathy. *Am. J. Respir. Crit. Care Med.* **2024**, *209* (2), 206−218.
(14) Wang, R. R.; Yuan, T. Y.; Wang, J. M.; Chen, Y. C.; Zhao, J. L.; Li, M. T.; et al. Immunity and inflammation in pulmonary arterial hypertension: From pathophysiology mechanisms to treatment perspective. *Pharmacol. Res.* **2022**, *180*, 106238.
(15) Tang, S.; Liu, Y.; Liu, B. Integrated bioinformatics analysis reveals marker genes and immune infiltration for pulmonary arterial hypertension. *Sci. Rep.* **2022**, *12* (1), 10154.
(16) Jiang, C.-Y.; Wu, L.-W.; Liu, Y.-W.; Feng, B.; Ye, L.-C.; Huang, X.; He, Y.-Y.; Shen, Y.; Zhu, Y.-F.; Zhou, X.-L.; et al. Identification of ACKR4 as an immune checkpoint in pulmonary arterial hypertension. *Front. Immunol.* **2023**, *14*, 1153573.
(17) Qin, Y.; Yan, G.; Qiao, Y.; Wang, D.; Tang, C. Identification of hub genes based on integrated analysis of single-cell and microarray transcriptome in patients with pulmonary arterial hypertension. *BMC Genomics* **2023**, *24* (1), 788.
(18) Wang, W.; Jiang, Z.; Zhang, D.; Fu, L.; Wan, R.; Hong, K. Comparative Transcriptional Analysis of Pulmonary Arterial Hypertension Associated With Three Different Diseases. *Front. Cell Dev. Biol.* **2021**, *9*, 672159.
(19) Awad, K. S.; Wang, S.; Dougherty, E. J.; Keshavarz, A.; Demirkale, C. Y.; Yu, Z. X.; Miller, L.; Elinoff, J. M.; Danner, R. L. BMPR2 Loss Activates AKT by Disrupting DLL4/NOTCH1 and PPARγ Signaling in Pulmonary Arterial Hypertension. *Int. J. Mol. Sci.* **2024**, *25* (10), 5403.
(20) Vieceli Dalla Sega, F.; Fortini, F.; Aquila, G.; Campo, G.; Vaccarezza, M.; Rizzo, P. Notch Signaling Regulates Immune Responses in Atherosclerosis. *Front. Immunol.* **2019**, *10*, 1130.
(21) Nakano, T.; Fukuda, D.; Koga, J.; Aikawa, M. Delta-Like Ligand 4-Notch Signaling in Macrophage Activation. *Arterioscler., Thromb., Vasc. Biol.* **2016**, *36* (10), 2038−2047.
(22) Hu, Y.; Chi, L.; Kuebler, W. M.; Goldenberg, N. M. Perivascular Inflammation in Pulmonary Arterial Hypertension. *Cells* **2020**, *9* (11), 2338.
(23) Zhang, M.-Q.; Wang, C.-C.; Pang, X.-B.; Shi, J.-Z.; Li, H.-R.; Xie, X.-M.; Wang, Z.; Zhang, H.-D.; Zhou, Y.-F.; Chen, J.-W.; et al. Role of macrophages in pulmonary arterial hypertension. *Front. Immunol.* **2023**, *14*, 1152881.
(24) Meng, L.; Hu, S.; Wang, J.; He, S.; Zhang, Y. DLL4(+) dendritic cells: Key regulators of Notch Signaling in effector T cell responses. *Pharmacol. Res.* **2016**, *113* (Pt A), 449−457.
(25) Meng, L.; Bai, Z.; He, S.; Mochizuki, K.; Liu, Y.; Purushe, J.; et al. The Notch Ligand DLL4 Defines a Capability of Human Dendritic Cells in Regulating Th1 and Th17 Differentiation. *J. Immunol.* **2016**, *196* (3), 1070−1080.
(26) Mitra, S.; Devi, S.; Lee, M.-S.; Jui, J.; Sahu, A.; Goldman, D. Vegf signaling between Muller glia and vascular endothelial cells is regulated by immune cells and stimulates retina regeneration. *Proc. Natl. Acad. Sci. U. S. A.* **2022**, *119* (50), No. e2083277177.
(27) Pabois, A.; Pagie, S.; Gerard, N.; Laboisse, C.; Pattier, S.; Hulin, P.; et al. Notch signaling mediates crosstalk between endothelial cells and macrophages via Dll4 and IL6 in cardiac microvascular inflammation. *Biochem. Pharmacol.* **2016**, *104*, 95−107.
(28) Jia, D.; Bai, P.; Wan, N.; Liu, J.; Zhu, Q.; He, Y.; et al. Niacin Attenuates Pulmonary Hypertension Through H-PGDS in Macrophages. *Circ. Res.* **2020**, *127* (10), 1323−1336.
(29) Yaku, A.; Inagaki, T.; Asano, R.; Okazawa, M.; Mori, H.; Sato, A.; et al. Regnase-1 Prevents Pulmonary Arterial Hypertension Through mRNA Degradation of Interleukin-6 and Platelet-Derived Growth Factor in Alveolar Macrophages. *Circulation* **2022**, *146* (13), 1006−1022.

https://doi.org/10.1021/acsomega.4c04307
ACS Omega 2024, 9, 37923−37933